Pergamon

Acta mater. Vol. 47, No. 1, pp. 363–371, 1999

Printed in Great Britain
PII: S1359-6454(98)00313-9
1359-6454/99 $19.00 + 0.00

COMPARISON OF PHASE-FIELD AND POTTS MODELS FOR COARSENING PROCESSES

V. TIKARE[1]†, E. A. HOLM[1], D. FAN[1] and L.-Q. CHEN[2]

[1]Sandia National Laboratories, Albuquerque, NM 87185-1411, U.S.A. and [2]Pennsylvania State University, University Park, PA 16802, U.S.A.

(Received 6 March 1998; in revised form 8 April 1998; accepted 13 July 1998)

Abstract—We have compared the phase-field model to the Potts model for two coarsening processes, grain growth and Ostwald ripening, both in two-dimensions. The Potts model is a discrete, statistical mechanical numerical simulation technique. In contrast, the phase-field model is a continuum, thermodynamic numerical simulation technique. The similarities and differences in microstructures, kinetics, and grain size distributions obtained for grain growth and Ostwald ripening by the phase-field model and by the Potts model were investigated. Both models gave very similar kinetic, topological and grain size distribution results for grain growth and Ostwald ripening in spite of their different approaches. In this paper, we review each model and its application to coarsening processes, present the results of grain growth and Ostwald ripening and finally, discuss how the physics of grain growth and Ostwald ripening is incorporated into these two different models. © *1998 Acta Metallurgica Inc. Published by Elsevier Science Ltd. All rights reserved.*

1. INTRODUCTION

Microstructural features control the properties and performance of engineering components to a large extent. Thus, it is vital that engineers tailor the microstructures of the components they fabricate to the components' applications. However, controlling microstructural evolution during processing is a challenging problem because of the large number of variables that must be understood and controlled. Therefore, predictive modeling techniques are necessary for tailoring microstructures to their applications.

Coarsening models are the most numerous and most mature of the microstructural evolution models. Many investigators have used a number of different numerical techniques to simulate coarsening by processes such as grain growth and Ostwald ripening. Among the numerical models used are the Potts model [1, 2], the phase-field model [3–5], front tracking model [6–8], Voronoi tessellation [9], and vertex model [10]. While each of these models is vastly different in how it incorporates the physics of coarsening, they all give similar results. Among these models, the Potts and phase-field [11, 12] are the arguably the most robust and versatile and certainly the most highly developed and widely applied.

The Potts model was first proposed by Potts as a generalization of the Ising model for simulating the critical transitions in magnetic materials with more than two degenerate states [13]. The Potts model treats the evolution of a nonequilibrium, discrete ensemble which populates a regular lattice. The ensemble can represent the composition and structure of materials. In the early 1980s, when computational facilities became sufficiently inexpensive to make it readily accessible, the Potts model was applied to coarsening phenomena, namely grain growth [1] and soap froth coarsening [2]. Since then, it has been modified to study many microstructural evolution problems including normal [14] and abnormal grain growth [15], recrystallization [16], coarsening in two phase systems, Ostwald ripening [17], and microstructural evolution in static [18] and dynamic thermal gradients [19]. The phase-field model [20] is based on the early field theory models [21] that in turn are based on the Cahn–Hilliard equation for a diffuse interface [22]. In contrast to the Potts model, the phase-field model employs parameters called field variables to represent microstructure. These field variables are continuum functions of spatial coordinates r and time t and are used to characterize a heterogeneous state consisting of phases with different composition and/or structure. Typical examples of these field variables can be the continuous fields of composition and long-range order parameters that characterize structural heterogeneities of a system. The evolution of these field variables in space with time gives the detailed information about the metastable and unstable microstructural states, which occur during microstructural evolution. The combination of developments in the numerical techniques and computation power has allowed many investigators to develop the phase-field model to study a wide variety of microstructural evolution

†To whom all correspondence should be addressed.

processes and progressively more complex problems. Some of these applications have been normal grain growth [3, 4], Ostwald ripening [23], combined grain growth and Ostwald ripening [24], microstructural evolution with coherent strain [25–27], twin formations [28, 29] and ferroelectric domain switching [30].

In this investigation, we will compare the Potts model to the phase-field model for two coarsening processes, grain growth and Ostwald ripening. The Potts model is a discrete, statistical–mechanical model; whereas, the phase-field model is a continuum, thermodynamic model. We will model normal grain growth under conditions as similar as the two very different models will permit, and compare kinetics and topological results. We will also model Ostwald ripening in a fully wetting, isotropic system under similar conditions using both models and compare the kinetics and grain size distribution results.

2. GRAIN GROWTH SIMULATIONS

2.1. Model description

Microstructure is represented in the Potts model by populating a lattice with a canonical ensemble as shown in Fig. 1. We use a square lattice and each lattice site is occupied by a "spin".† Contiguous sites of the same spin form a grain with a sharp grain boundary between adjacent grains. The spin occupying each lattice site maybe conceptualized as a discrete quantity of matter on the scale of billions of atoms of the same state. The number of different, degenerate spins that the lattice sites can assume is Q. The individual state is designated by the symbol q and the total number of states in the system is Q, $q_{\text{grain}} = [1, 2, \ldots, Q]$. The equation of state defining the energy for these simulations is the sum of all the neighbor interaction energies in the system given by

$$E = \frac{1}{2}\sum_{i=1}^{N}\sum_{j=1}^{8} E_{q_i q_j} \tag{1}$$

where N is the total number of sites, q_i is the state of the grain at site i, q_j is the state of the nearest neighbor at site j and $E_{q_i q_j}$ is the neighbor interaction energy between neighbors located at site i and j. In the grain growth simulations, for $q_i = q_j$ the interaction energy $E_{q_i q_j} = 0$ and for $q_i \neq q_j$ the interaction energy $E_{q_i q_j} = 1.0$. Thus, the only energy considered in the simulation is the interfacial energy and all unlike neighbors contribute one arbitrary unit of energy to the system. This yields a single-component, single-phase system with uniform, isotropic [31] interfacial energies between grains.

†The term spin originates from the original application of the Potts model which was to study phase transitions in magnetic materials.

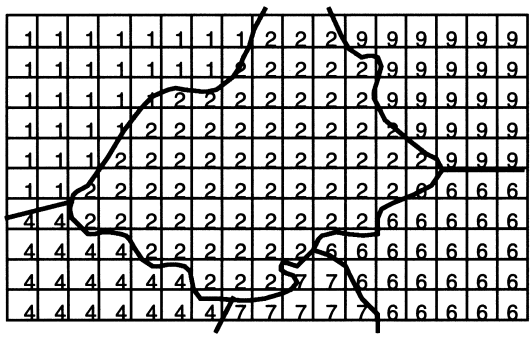

Fig. 1. Microstructure representation in the Potts model. Each integer occupying a lattice site is a spin and contiguous spins of the same value form a grain.

Now that the microstructural representation and system energies are defined in the simulation, we turn to the grain growth mechanism. Grain growth is simulated using the method developed in previous works [1, 31]. First, a grain site is chosen at random from the simulation space. Then a new state q is chosen at random from the Q possible states in the system. The grain site is temporarily assigned the new state and the change in energy is evaluated using equation (1). Next the standard Metropolis algorithm is used to perform the grain growth step based on Boltzmann statistics. A random number, R, between 0 and 1 is generated. Next, the transition probability, P, is calculated using

$$P = \begin{cases} \exp\left(\dfrac{-\Delta E}{k_{\text{B}} T}\right) & \text{for } \Delta > 0 \\ 1 & \text{for } \Delta E \leq 0 \end{cases} \tag{2}$$

where k_{B} is the Boltzmann constant and T is temperature. If the $R \leq P$, then the grain growth step is accepted, if not, the original state is restored. The simulation temperature used for grain growth was $k_{\text{B}}T = 0$ and has been shown to simulate grain growth well [31]. Time in the Potts model is measured in units of Monte Carlo step; 1 MCS corresponds to N attempted changes where N is the total number of sites in the system.

The phase-field model is a thermodynamic model, which uses a field representation for microstructure. A continuum grain and grain boundary structure is mapped onto a discrete, square, lattice using a set of order parameters, $\{\eta_i(\text{r})\}$ where $i = \{1, 2, \ldots, P\}$, which may be conceptualized as membership of site r in P different grains. This set of order parameters is allowed to evolve with time at each lattice point r to simulate microstructural evolution. Figure 2 is a schematic diagram showing how the order parameters vary continuously from one grain to its neighbor to form diffuse grain boundaries. For the grain interior site, all order parameters have values of 0.0 except one; it has a value of 1.0.

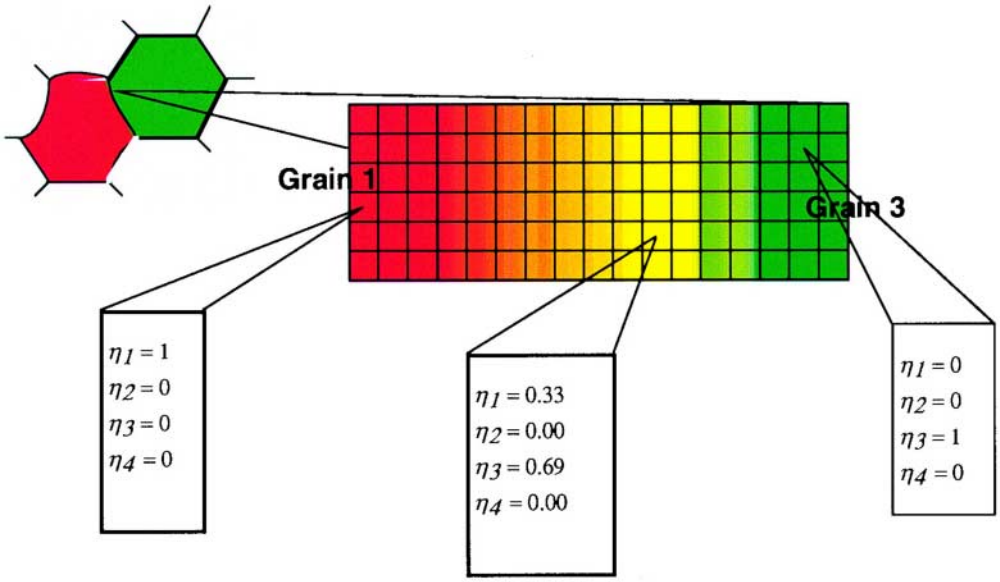

Fig. 2. Microstructural representation of the phase-field model.

This may be interpreted as that site having exclusive and full membership in the grain represented by that particular order parameter and in no other grains. A site at an interface between two grains, has partial membership in the two grain on either side of it and no membership in any other grains. The order parameters are nonconserved parameters, thus they need not sum to any particular value locally at any given site or globally at all sites. This type of representation leads to diffuse interfaces as described by Cahn and Hilliard [22].

The equation of state for the simulation is a free energy function, F, which is a function of the order parameters. It defines the energy of the system given any combination of order parameters η_is. The order parameters, η_is, are locally and globally nonconserved parameters. Since the free-energy is defined for all possible combination of η_is, the combination of these parameters which gives the lowest F is the equilibrium state of the system.

The free energy for the system studied here was defined as

$$F = \int \left[f_0(\eta_1(r), \ldots, \eta_p(r)) + \sum_{i=1}^{p} \frac{\kappa_i}{2} (\nabla \eta_i + (r))^2 \right] \mathrm{d}^3 r \qquad (3)$$

where f_0 is the bulk chemical free energy,

$$f_0 = -\frac{\alpha}{2} \sum_{i=1}^{p} \eta_i^2 + \frac{\beta}{4} \left(\sum_{i=1}^{p} \eta_i^2 \right)^2 + \left(\gamma - \frac{\beta}{2} \right) \sum_{i=1}^{p} \sum_{j \neq i}^{p} \eta_i^2 \eta_j^2 \qquad (4)$$

with $\alpha = 1$, $\beta = 1$ and $\gamma = 1$.

In this model, the interfacial energies are introduced by the excess free energy in the interface and by gradients in the order parameters, $2\kappa_i(\nabla \eta_i)^2$, where κ_i are the gradient coefficients of the order parameters. Thus, at grain boundaries and triple junctions where order parameters change spatially, the free energy of the system is increased.

The driving force for microstructural evolution is the reduction of total free energy of a system. In this case, the total interfacial energy is decreased as the microstructure evolves. Kinetics for microstructural evolution is introduced by the time-dependent Ginzburg–Landau equations.

$$\frac{\mathrm{d}\eta_i(r,t)}{\mathrm{d}t} = -L_i \frac{\delta F(r,t)}{\delta \eta_i} = -L_i \frac{\partial f_0(r,t)}{\partial \eta_i} + L_i \kappa_i \nabla^2 \eta_i(r,t) \qquad (5)$$

where L_i is the kinetic rate coefficient related to interface mobility and diffusivity. Equation (6) determines the evolution of the order parameters and hence the grain structure.

The starting microstructures for this study was initialized by assigning small random numbers between –0.001 and 0.001 for each order parameter at each site at time $t = 0.0$. This microstructure is analogous to a supercooled liquid. Once the microstructure is initialized, grain growth is simulated by repetitive calculation of order parameters at each site for the next time increment $t = t + \Delta t$ or $\eta_i(r, t + \Delta t)$ which is calculated using the forward Euler technique,

$$\eta_i(r, t + \Delta t) = \eta_i(r,t) + \frac{\partial \eta_i(r,t)}{\partial t} \Delta t \qquad (6)$$

where the quantity $\partial \eta_i / \partial t$ is determined using

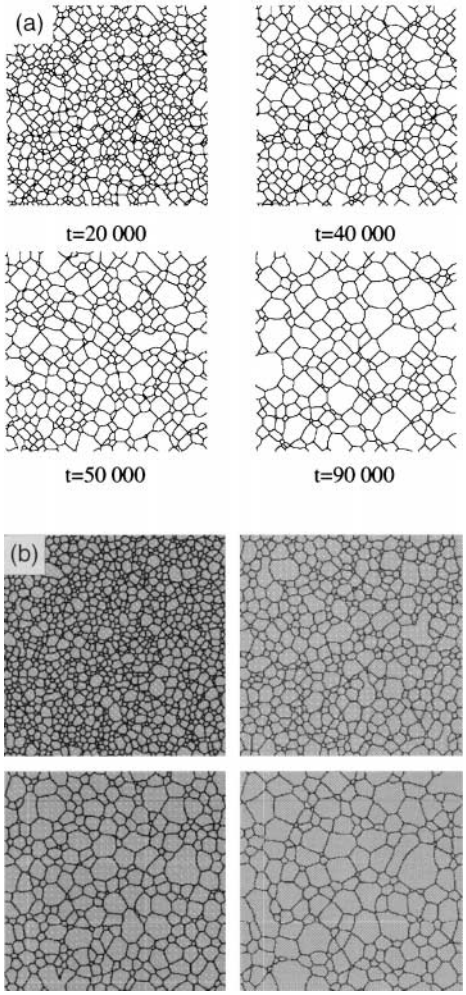

Fig. 3. Grain growth microstructures resulting from the (a) Potts model and (b) the phase-field model at various times.

equation (5). The Laplacians used in equation (5) were calculated for a discretized system as

$$\nabla^2\eta = \frac{1}{(\Delta x)^2}\left[\frac{1}{2}\sum_i(\eta_i - \eta_r) + \frac{1}{4}\sum_j(\eta_j - \eta_r)\right] \quad (7)$$

where Δx is the grid size, i is the set of first nearest neighbors of site r, and j is the set of second nearest neighbors of site r.

2.2. Comparison of results

The resulting grain growth microstructures from the Potts model and phase-field model simulations are shown in Fig. 3(a) and (b). The microstructures for the two simulations look very similar. Both simulations were run on a square lattice with first and second nearest neighbor interactions and with the same degeneracy of $Q = 72$ in the Potts model and $P_\eta = 36$ with each η assuming positive and negative values for a total of 72 states in the phase-field model. While, the microstructures shown in Fig. 3(a) and (b) look very similar, the Potts model grains have sharp grain boundaries between adjacent lattice sites, in contrast to the phase-field model grains which have diffuse grain boundaries which extend on average over 7 lattice sites. Previous work has shown that the grain growth kinetics in both models is in agreement with the predictions of grain growth theory, giving a grain growth exponent of $n = 2$ in the following relationship:

$$R^n = Kt \quad (8)$$

where R is the average grain radius, t is time and K is a proportionality constant.

The grain size distributions obtained from the two models is plotted Fig. 4. The two distributions are in good agreement with each other, well within

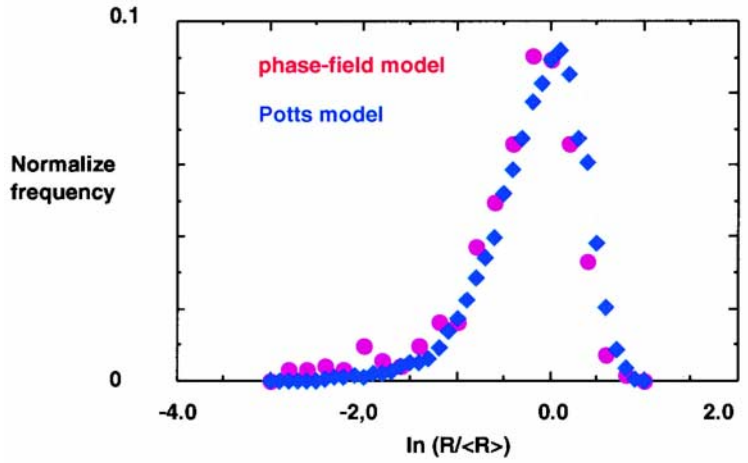

Fig. 4. Grain size distributions obtained from the phase-field model and Potts model grain growth simulations.

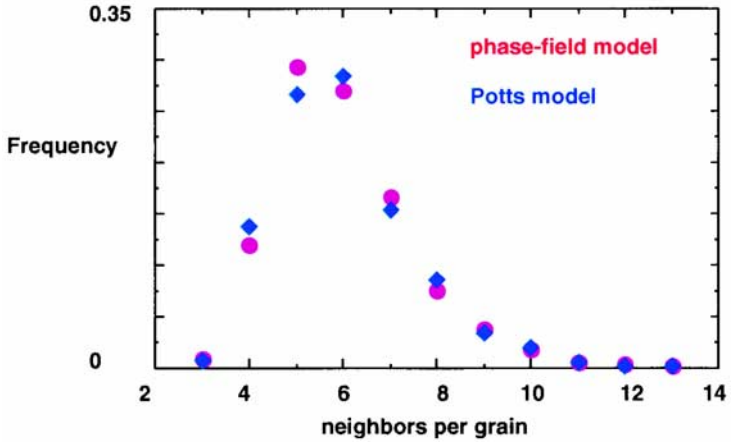

Fig. 5. Topological results obtained from the phase-field and Potts model grain growth simulations.

statistical error. The range of grain sizes agrees well. The peak in grain size distribution from the phase-field model is shifted slightly to the smaller grain sizes. This may be because the grain area is slightly under estimated as the grain boundary regions have a finite thickness in the phase-field model. The topological results, distribution of the number of neighboring grains of all grains, are compared in Fig. 5. Again, there is good agreement, well within the statistical error. The peak of the neighbor distribution curve obtained from the phase-field model is shifted to fewer neighbors with respect to the Potts model neighbor distribution curve. This is attributed to the fact that as the small grains in the phase-field representation shrink, they approach the resolution of the grain boundary region and "disappear" prematurely. Overall, there is excellent agreement between the grain growth results of the two models.

3. OSTWALD RIPENING SIMULATIONS

3.1. Model description

The Potts model described in the previous section on grain growth was modified to represent a two-component, two-phase system necessary to simulate Ostwald ripening. Two types of spins were used; one type was a set of spins, $q_A = \{1, 2, \ldots, 100\}$ used for the solid grain phase and the other type was just one spin $q_B = -1$ for the liquid matrix. The equation of state used for Ostwald ripening is given by equation (1) with neighbor interaction energies defined as $E_{q_A q_A} = 2.5$ for dissimilar q_As, and $E_{q_A q_B} = 1.0$ resulting in two different interfacial energies, solid–liquid interfacial energy defined by $E_{q_A q_A}$ and solid–solid grain boundary energy defined by $E_{q_A q_A}$. The use of two types of spins and the two energies resulted in a two-component, two-phase system necessary for the simulation of Ostwald ripening [32]. The mechanism for microstructural evolution by Ostwald ripening was simulated by choosing a site i at random and then choosing a neighboring site j also at random. If one site is an A-site and the other a B-site, then the two are temporarily exchanged with the A-site assuming one of the 100 possible states at random. The change in energy for this exchange is evaluated and the standard Metropolis algorithm with the transition probability given in equation (2) was used to determine if the exchange is accepted or rejected.

The phase-field model described previously was also modified to describe a two-phase, two-component system. This was done by using a set of order parameters, $\eta_i(r,t)$, which distinguish the different orientations of solid grains, and by introducing a concentration field variable, $C(r,t)$, which takes the value of C_α within the liquid phase and C_β within a solid phase grain. All order parameters (orientation field variables) are zero in the liquid phase. At the solid–liquid interface the order parameters would transition from 1.0 to 0.0 and the composition from C_β to C_α. The total free energy of the two phase system would be the function of $\eta_i(r,t)$ and $C(r,t)$:

$$F = \int \left[f_0(C(r);\eta_1(r),\eta_2(r),\ldots,\eta_p(r)) + \frac{\kappa_C}{2}(\nabla C(r))^2 + \sum_{i=1}^{p} \frac{\kappa_i}{2}(\nabla \eta_i(r))^2 \right] \mathrm{d}^3 r \quad (9)$$

with the following chemical free energy:

$$f_0 = f_1(C) + \sum_{i=1}^{p} f_2(C,\eta_i) + \sum_{i=1}^{p}\sum_{j\neq i}^{p} f_3(\eta_i,\eta_j) \quad (10)$$

in which

$$f_1(C) = -(A/2)(C - C_m)^2 + (B/4)(C - C_m)^4 + (D_\alpha/4)(C - C_\beta)^4$$

$$f_2(C,\eta_i) = -(\gamma/2)(C - C_\alpha)^2(\eta_i)^2 + (\delta/4)(\eta_i)^4$$

$$f_3(\eta_i,\eta_j) = (\epsilon_{ij}/2)(\eta_i)^2(\eta_j)^2$$

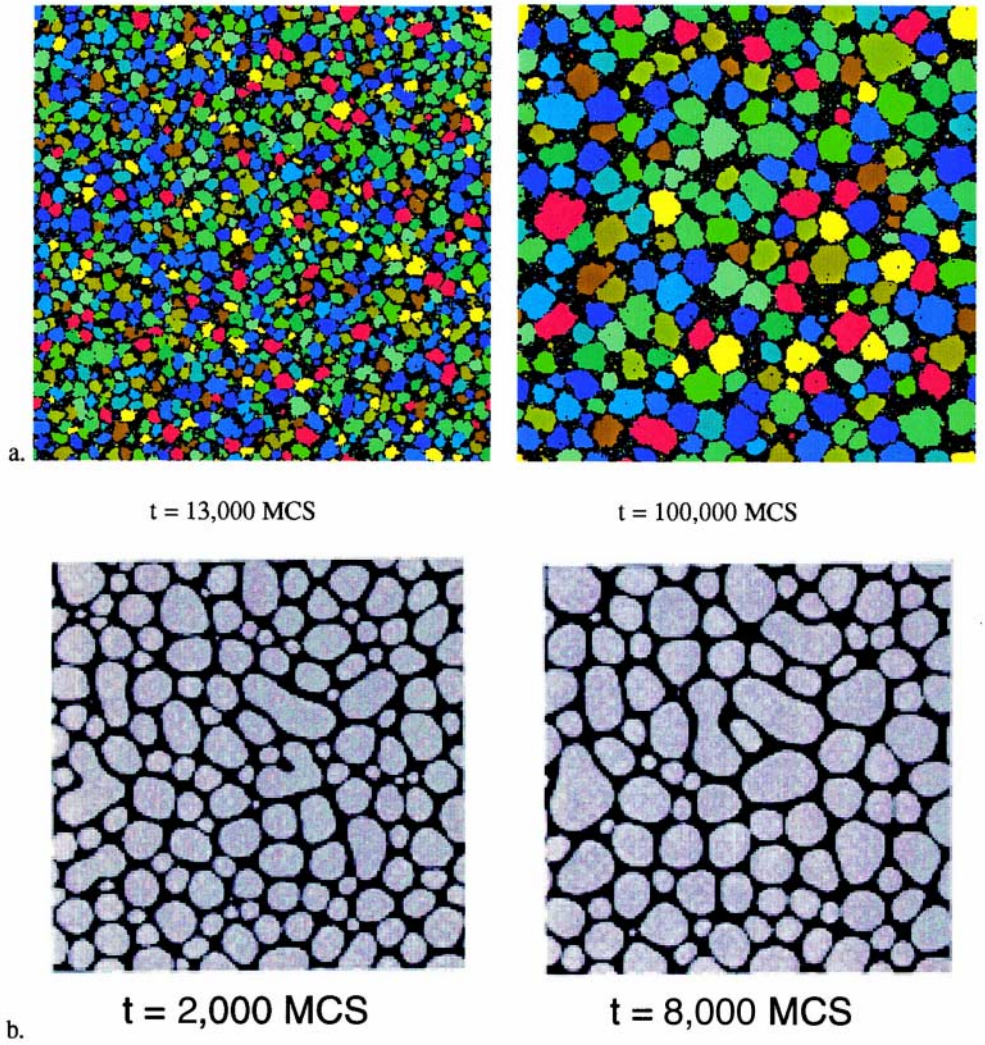

Fig. 6. Microstructures obtained from (a) Potts and (b) phase-field model simulations of Ostwald ripening.

with $C_\alpha = 0.05$, $C_\beta = 0.95$, $C_m = (C_\alpha + C_\beta)/2 = 0.5$, $A = 2.0$, $B = 1.0$, $D_\alpha = D_\beta = 1.2$, $\gamma = 2.0$, $\delta = 1.0$, and $\epsilon = 3.0$. The gradient coefficients were chosen as: $\kappa_i = \kappa_j = \kappa_C = 2.0$. Microstructural evolution was driven by the minimization of free energy given in equation (9) and the kinetics are calculated using equation (6) where $\partial\eta/\partial t$ is given by the Ginzburg–Landau relationship of equation (5). The change in composition at each site is also given by the Ginzburg–Landau relationship for conserved parameters

$$\frac{\partial C}{\partial t} = \nabla\left(L_C \nabla \frac{\delta F}{\delta C(r,t)}\right) = L_C\left\{\nabla^2\left(\frac{\partial f}{\partial C} - \kappa_c \nabla^2 C\right)\right\}. \quad (11)$$

The forward Euler technique is used to calculate the composition C at the next time step.

3.2. Results

The microstructures resulting from the Ostwald ripening simulation of the Potts model and phase-field model are shown in Fig. 6(a) and (b), respectively. Both models show equi-axed grains dispersed in a matrix. The phase-field model has grains which are regular and smooth where as the Potts model has irregular, but equi-axed grains. These features are due to the nature of the two models. The phase-field model maps continuum fields on to a lattice giving smooth regular features. The Potts model is a statistical–mechanical model which samples a number of configurations favoring the lower energy ones, thus the irregular appearance. A few of the grains in the phase-field microstructure have slightly elongated appearance due to coalescence. Coalescence is two or more neighboring grains fusing together to form one grain. Coalescence is expli-

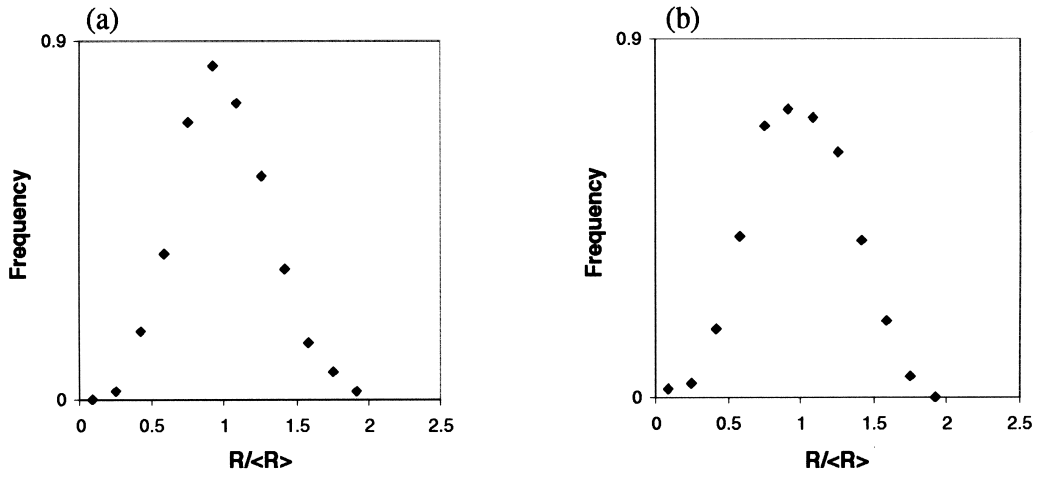

Fig. 7. Grain size distributions obtained from the Potts model for Ostwald ripening at grain fraction (a) 0.89 and (b) 0.41.

citly prohibited in the Potts model simulations, so all the grains are equi-axed.

Ostwald ripening theories predict a grain growth exponent of $n = 3$ for diffusion limited kinetics as formalized by

$$R^n = Kt \tag{12}$$

where R is the average grain radius, K is a rate constant and t is time. Both the Potts and the phase-field model gave grain growth kinetics with grain growth exponents of $n = 3$ and is described in detail elsewhere [17, 23, 33].

Self-scaling of the microstructure was achieved in both sets of simulations as predicted by Ostwald ripening theories. The grain size distributions in the self-scaling region from the two models, shown in Figs 7 and 8, at different volume fraction of solids are in good agreement. The skewness of both grain size distributions at the high grain fractions is to the larger grain sizes. As grain fraction decreases, the skewness in both sets of grain size distributions changes to smaller sizes. While the trends are similar, direct comparison of the two models is inappropriate because of the few coalescence events seen in the phase-field simulations which change the grain size distributions slightly. Again, very similar results were obtained from the two models for Ostwald ripening.

4. DISCUSSION

Grain growth is a capillarity driven phenomenon with short range diffusion across grain boundaries. The two models, Potts and phase-field, simulate capillarity and grain boundary migration by short range diffusion using very different approaches. Capillary forces require an interface with an associated energy and curvature of the interface. The Potts model, at any given instant, has a sharp interface between neighboring sites. The broken bonds between neighboring sites contribute to the interfacial energy. Furthermore, the interface is discretized around the lattice site with curvature also being discretized in line segments of length equal to the lattice site dimension. The phase-field model has diffuse grain boundaries which are several lattice

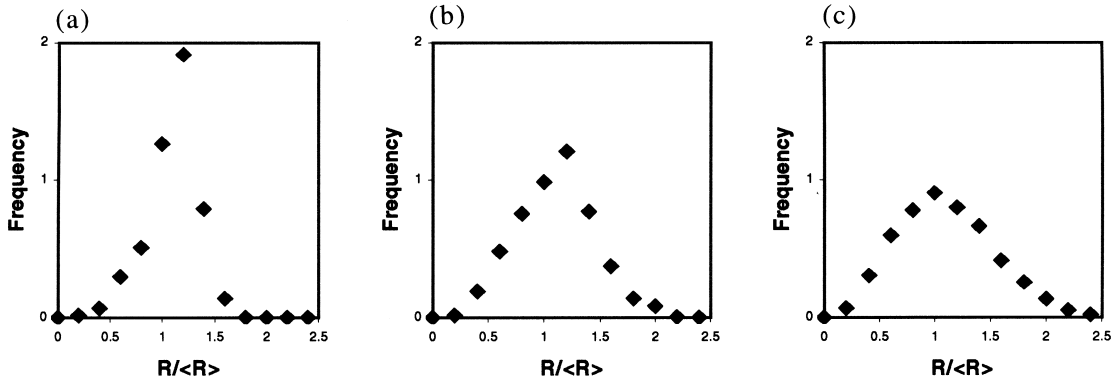

Fig. 8. Grain size distributions obtained from the phase-field model for Ostwald ripening simulations at grain fraction (a) 0.25, (b) 0.50 and (c) 0.90.

sites wide. The interfacial energy is due to the excess free energy of the grain boundary and the gradient energy as defined in equation (5). In the phase-field model, the interface itself is a smooth continuously curving grain boundary rather than a discretized one seen in the Potts model.

These interfaces move in response to diffusion across the grain boundary driven by curvature. Diffusion is also simulated very differently by the two simulation methods. The Potts model simulates diffusion across the grain boundaries by the "spin flip" method which may be visualized as discrete quanta of material at the grain boundary changing to the neighboring grain. Thus, as a result of a spin flip event the grain boundary jumps by a lattice dimension. In contrast, the phase-field model simulates grain boundary migration as a smoothly moving interface driven by curvature. The order parameters, $\eta_i(r,t)$, vary continuously across the grain boundary both in space and time to simulate a continuously moving, diffuse grain boundary.

To simulate Ostwald ripening, two additional phenomena must be simulated, the Gibbs–Thomson effect and diffusion in the matrix phase. Again the two models simulated these differently. The Gibbs–Thomson effect was simulated automatically in the Potts model because the probability of sites detaching at the grain–matrix interface was greater for smaller grains than for larger grains. Diffusion through the matrix phase in the Potts model is simulated by random walk of single A-sites in the matrix. A net flux from smaller grains to larger grains is achieved due to the Gibbs–Thomson effect. In the phase-field model, the Gibbs–Thomson effect was implicitly included in the free energy formulations. The chemical potential outside a small grain is higher than that outside a large grain, thus making the solution concentration in the matrix surrounding the smaller grains higher than that in the matrix surrounding the larger ones. Diffusion in the matrix results due to the difference in solution concentration between small and large grains. In the phase-field model, diffusion is governed by equation (11) which reduces to Fick's first law of diffusion when chemical potential within solid grains and liquid far from interfaces are in equilibrium.

Another difference between these two models is that the phase-field model is a deterministic model. Once the initial starting microstructure is defined, the microstructural evolution is completely deterministic if thermal noise is not considered in the simulations. The Potts model on the other hand, is a stochastic model, it gives statistically similar results, but not duplicate microstructures.

The Potts model is a discrete model which utilizes a statistical–mechanical ensemble which evolves with given mechanisms to simulate microstructural evolution. When the ensemble is large, a large number of ensemble configurations can be sampled with probabilities corresponding to their configurational energy to simulate microstructural evolution accurately. The ensemble configurations include ones discussed in this paper for coarsening processes such as grain boundary curvature and mobility, solution, precipitation, and diffusion by random walk. In contrast, the phase-field model maps a continuum field on to a discrete lattice with the continuum quantities which are explicitly incorporated into the model. The energies and kinetics of microstructural evolution in the phase-field model are the integral values of the discrete events in the Potts model. Consider the grain boundary; its energy is explicitly defined by equation (3) for a given set of order parameters and curvature of the boundary will increase the grain boundary energy. The mobility of the grain boundary is again explicitly incorporated into the phase-field model by equation (5). Likewise, solution characteristics are given by equation (10) and the diffusion of the components making up the solution phase by equation (11). When the Potts model is properly applied by sampling a large ensemble with the appropriate configurations, it will in the limit of large ensemble size and sampling frequency approximate the continuum behavior of the phase-field model.

5. CONCLUSIONS

We have shown that despite their fundamentally different approaches, the Potts and phase-field model give similar results for two coarsening processes, grain growth and Ostwald ripening. The Potts model simulates coarsening by the evolution of a mesoscale ensemble with specific statistical–mechanical characteristics and mechanisms for evolution. When these are applied over a sufficiently large ensemble and many computation steps, the Potts model simulated the continuum thermodynamic and kinetic characteristic which are explicitly incorporated into the phase-field model. This is shown by the fact that microstructures, kinetics, grain growth topology and grain size distribution obtained from both models were very similar for two coarsening processes.

REFERENCES

1. Anderson, M. P., Srolovitz, D. J., Grest, G. S. and Sahni, P. S., *Acta metall.*, 1984, **32**, 783.
2. Wejchert, J., Weaire, D. and Kermode, J. P., *Phil. Mag. B*, 1986, **53**, 15.
3. Fan, D. and Chen, L.-Q., *Acta mater.*, 1997, **45**, 611.
4. Fan, D. and Chen, L-A., *Acta mater.*, 1997, **45**, 1115.
5. Chen, L.-Q. and Yang, W., *Phys. Rev. B*, 1994, **50**, 15752.
6. Frost, H. J., Thompson, C. V., Howe, C. L. and Whang, J., *Scripta metall.*, 1988, **22**, 65.
7. Chaix, J. M., Guyon, M., Rodriguez, J. and Allibert, C. H., *Scripta metall.*, 1988, **22**, 71.

8. Fortes, M. A. and Ferro, A. C., *Acta metall.*, 1985, **33**, 1697.
9. Mahis, K. W., Hanson, K. and Morrid, J. W. Jr, *Acta metall.*, 1980, **28**, 443.
10. Marsh, S. P., Masumura, R. A. and Pande, C. S. nde, *Phil. Mag. Lett.*, 1995, **72**, 429.
11. Chen, L.-Q. and Wang, Y., *JOM*, 1996, **48**, 12.
12. Fan, D. and Chen, L.-Q., *Acta mater.*, 1997, **45**, 3297.
13. Wu, F. Y., *Rev. Mod. Phys.*, 1982, **54**, 235.
14. Anderson, M. P., Grest, G. S. and Srolovitz, D. J., *Phil. Mag. B*, 1989, **59**, 293.
15. Srolovitz, D. J., Grest, G. S. and Anderson, M. P., *Acta metall.*, 1985, **33**, 2233.
16. Srolovitz, D. J., Grest, G. S., Anderson, M. P. and Rollett, A. D., *Acta metall.*, 1988, **36**, 2115.
17. Tikare, V. and Cawley, J. D., *Acta metall.*, 1998, **46**, 1333.
18. Tikare, V. and Holm, E. A. *J. Am. Ceram. Soc.* 1998, **81**.
19. Tikare, V., Griffith, M. L., Schlienger, E. and Smugeresky, J., in *Solid FreeForm Fabrication Symposium 1997*, ed. D. Borell, J. Hymen, H. Marcus and J. Barlow. Jenny's Printing, 1997.
20. Chen, L.-Q. and Wang, Y., *JOM*, 1996, **48**, 13.
21. Gunton, J. D., San Miguel, M. and Sahni, P. S.. in *Phase Transitions and Critical Phenomena*, Vol. 8, ed. C. Domb and J. L. Lebowitz. Academic Press, New York, 1983, p. 287.
22. Cahn, J. W. and Hilliard, J. E., *J. Chem. Phys.*, 1958, **28**, 258.
23. Fan, D., Chen, L.-Q., Chen, S. P. and Voorhees, P. W., *Comput. Mater. Sci.*, in press.
24. Fan, D. and Chen, L.-Q., *J. Am. Ceram. Soc.*, 1997, **80**, 1773.
25. Chen, L.-Q., Wang, Y. and Khachaturyan, A. G., *Phil. Mag. Let.*, 1991, **64**, 241.
26. Wang, Y., Wang, H., Chen, L.-Q. and Khachaturyan, A. G., *J. Am. Ceram. Soc.*, 1993, **76**, 3029.
27. Wang, Y., Wang, H., Chen, L.-Q. and Khachaturyan, A. G., *J. Am. Ceram. Soc.*, 1995, **78**, 657.
28. Fan, D. and Chen, L.-Q., *J. Am. Ceram. Soc.*, 1995, **78**, 769.
29. Fan, D. and Chen, L.-Q., *J. Am. Ceram. Soc.*, 1995, **78**, 1680.
30. Yang, W. and Chen, L.-Q., *J. Am. Ceram. Soc.*, 1995, **78**, 2554.
31. Holm, E. A., Glazier, J. A., Srolovitz, D. J. and Grest, G. S., *Phys. Rev. A*, 1991, **43**, 2662.
32. Tikare, V. and Cawley, J. D., *J. Am. Ceram. Soc.*, 1998, **81**.
33. Tikare, V. and Cawley, J. D., *Acta metall.*, 1998, **46**, 1443.